Additive Manufacturing 28 (2019) 719–726

Contents lists available at ScienceDirect

Additive Manufacturing

journal homepage: www.elsevier.com/locate/addma

Full Length Article

Nozzle-integrated pre-deposition and post-deposition heating of previously deposited layers in polymer extrusion based additive manufacturing

Darshan Ravoori, Hardikkumar Prajapati, Viswajit Talluru, Ashfaq Adnan, Ankur Jain*

Mechanical and Aerospace Engineering Department, University of Texas at Arlington, Arlington, TX, USA

ARTICLE INFO

Keywords:
Additive manufacturing
Polymer extrusion
Heat transfer
Thermal diffusion
Infrared thermometry
Interlayer bonding

ABSTRACT

The adhesion and merging of adjacent filaments in polymer extrusion based additive manufacturing (AM) plays a key role in determining the thermal and mechanical properties of the built part. It is well known that maintaining the deposited filaments at a high temperature aids in the process of adhesion and merging. While external mechanisms such as laser and infrared heating have been used in the past to heat up deposited filaments, this paper presents a simpler, less invasive and *in situ* mechanism for heating of previously deposited layers using a hot metal block integrated with and rastering together with the filament-dispensing nozzle. Infrared thermography based quantitative measurement of temperature field along the raster line is carried out for two configurations – a preheater and a postheater traveling ahead of or behind the nozzle respectively. In each case, significant temperature rise in the deposited filaments is shown. A configuration comprising both preheater and postheater is shown to result in additional thermal benefits. The measured temperature rise is shown to be a function of process parameters such as raster speed and heater-to-base gap. Experimental measurements are shown to agree well with theoretical and simulation models. Cross-section imaging of samples printed without and with the *in situ* heating clearly show significant improvement in neck growth and filament-to-filament merging compared to the baseline case. Improvement in thermal and structural performance of printed samples is also demonstrated. Compared to other techniques proposed in the past, the heating approach presented in this work is passive and requires minimal additional costs or complexity. The improved temperature field and consequently enhanced filament adhesion reported here may help design and build parts with superior thermal and mechanical properties using polymer AM.

1. Introduction

Additive manufacturing (AM) has been widely investigated due to several key advantages offered over traditional manufacturing approaches. AM enables rapid manufacturing of complicated geometries that were difficult or impossible to build with traditional manufacturing [1,2]. This increased manufacturability has offered a significantly expanded design space for components [3,4]. While early work on AM focused on building models and prototypes, it is now increasingly being used for building multifunctional parts expected to bear mechanical or thermal load [5–7].

Given the increased recent interest in additively manufactured multifunctional parts, the thermal and mechanical properties of additively manufactured parts, and the impact of process parameters on these properties has been studied extensively [6–11]. The polymer AM process involves the dispensing of a filament that is heated to a temperature greater than the glass transition temperature or melting temperature, for amorphous and semi-crystalline polymers, respectively. Following deposition, adjacent filaments merge into each other while cooling down. As the temperature approaches the glass transition temperature, the polymer becomes extremely viscous, thereby stopping neck growth between filaments [12,13]. The thermally-driven neck growth and merging between filaments is the fundamental process that imparts mechanical strength and good thermal conductivity to the part [7,9,10]. Experiments have shown that maintaining previously deposited layers at a high temperature results in improved inter-layer bonding [14,15]. As a result, heat transfer during the filament deposition process is important to understand and optimize.

Research on experimental and theoretical/numerical investigation of heat transfer during polymer AM has been presented in the past. Heat transfer modeling of the AM process has been carried out with varying degrees of detail, including one-dimensional [16] and three-dimensional analytical modeling [17], finite-element simulations [11,18], etc. Infrared thermometry based measurements of temperature distribution

* Corresponding author at: 500 W First St, Rm 211, Arlington, TX, 76019, USA.
E-mail address: jaina@uta.edu (A. Jain).

https://doi.org/10.1016/j.addma.2019.06.006
Received 23 January 2019; Received in revised form 30 May 2019; Accepted 6 June 2019
Available online 07 June 2019

in the stand-off gap [19] and around a deposited filament have been presented [17,20]. Temperature distribution around the deposited filament has been shown to be influenced by the thermal energy of the deposited filament, as well as heat transfer directly from the hot nozzle [17]. Through both experiments [7,17] and modeling [11,13], process parameters such as raster speed, filament diameter, etc. have been shown to play a key role in determining the rate of cooling of the filament. Both measurements and theoretical models show very rapid temperature drop in and around the filament, underscoring the critical need for optimizing heat transfer during polymer AM to ensure that the filament stays above glass transition temperature for as long as possible.

The important role played by temperature and heat transfer in determining the properties of the printed part is also highlighted by papers that investigate post-process thermal annealing [21–23]. A variety of experiments have reported significant enhancement in thermal and mechanical properties of polymer printed parts exposed to a high temperature for a certain time after printing. Both annealing time and temperature have been shown to influence such enhancement [21,22], which appears to occur due to improved filament-to-filament bonding when subjected to high temperature for a period of time.

Both sets of past work described above suggest the importance of maintaining a high temperature in and around the filament for as long as possible. Some possible process-related changes to enable this include increasing the nozzle temperature, reducing the thermal diffusivity of the filament material, maintaining the build chamber at a high temperature, etc. Clearly, there are practical limitations for these approaches, since, for example, thermal conductivity of the filament is fixed by the material choice, and the nozzle temperature can not be made too high because of undesirable changes in material properties at high temperature. Changing the raster speed is also unlikely to be effective, as this has been shown to not influence the peak temperature or rate of temperature reduction, and may actually inhibit neck growth between filaments [7].

A few approaches for external heating of the deposited filaments have been investigated in the past. For example, using an elaborate set of mirrors and other optics, a near-IR laser beam has been focused to provide local pre-heating prior to filament deposition [24]. An infrared lamp has also been used for preheating [25]. Microwave heating has been utilized for raising the local temperature during polymer AM [26]. These papers report increased local temperature and enhanced filament-to-filament adhesion due to localized heating. However, each of these approaches requires additional, expensive equipment and result in complications in the process flow. A passive approach for preheating of previously deposited layers is highly desirable.

One possible approach for increasing the time duration for which the deposited filament remains at high temperature is to provide an extended, hot surface that rasters along with the nozzle as shown schematically in Fig. 1(a). Past work has already shown that heat transfer from the hot nozzle surface influences temperature distribution on the previous deposited layers [17]. Consequently, the presence of a hot metal block that moves along with the nozzle may further increase temperature of previously deposited layers and keep the present layer at an elevated temperature for a longer time. Compared to other approaches investigated in the past, such as laser [24], infrared [25] and microwave [26] heating, this approach significantly reduces the physical distance between the heater and print bed (1–2 mm in the present work compared to around 8 cm in infrared heating [25]). As a result of the much lower gap, the heater provides adequate heating without needing to be maintained at a very high temperature such as an IR heater. Due to the tight integration with the nozzle, the present approach is relatively passive and easy to implement, since a heating mechanism, usually through Joule heating, is already being used to heat up the nozzle barrel and can be easily extended for the hot metal block without much added cost or complexity.

This paper presents experimental and theoretical analysis of the heating of previously deposited layers using a hot metal surface that rasters close to the base along with the dispensing nozzle. Two configurations are analyzed – a preheater configuration in which the hot metal surface rasters ahead of the nozzle, and a postheater configuration in which the hot metal surface rasters behind the nozzle. Temperature measurement based on infrared imaging is carried out. As expected, the preheater and postheater configurations result in significant temperature increase before and after filament dispense respectively. A configuration with both preheater and postheater is also analyzed. The extent of temperature increase is found to be a strong function of the gap between heater and bed surface, as well as the raster speed. Experimental data are found to be in good agreement with a mesh deformation based finite-volume simulation model. Cross-section imaging of printed parts clearly shows significant impact of this approach on filament-to-filament neck growth. Enhancement in thermal and mechanical properties is demonstrated.

Section 2 describes the experimental setup for integrating preheater and postheater configurations into the polymer AM process as well as infrared thermography measurements. Theoretical and finite-volume simulation modeling is discussed in section 3. Key results are presented and discussed in Section 4.

2. Experiments

Experiments are carried out to measure the thermal effect of preheating and postheating configurations during filament dispensing process. Temperature along the raster line is measured as a function of time using an infrared camera. Fig. 2(a) and 2(b) show pictures of the experimental setup, comprising a custom-built Anet A8 3D printer, a FLIR A6703sc InSb infrared camera and a 6 mm thick poly-lactic acid (PLA) sample on which filaments are deposited. The Aluminum build plate dimensions are 200 mm by 200 mm. Stepper motors for x, y and z movement are controlled by an A-1284 mainboard. The geometry to be printed is modeled in a CAD software and converted to G-code using Simplify3D software. 1.75 mm diameter TrueBlack color PLA filament from Makerbot is fed into the nozzle block, heated up and dispensed through a 0.4 mm brass nozzle. Filament feedrate is determined by Simplify3D software based on process parameters such as print speed and layer height in order to maintain consistent flowrate.

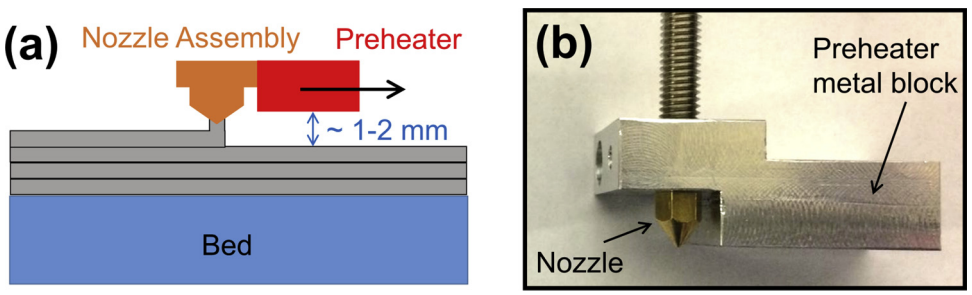

Fig. 1. (a) Schematic of nozzle-integrated hot surface based preheating. Note the raster direction. If reversed, the preheater effectively acts as a postheater. Not to scale. (b) Picture of preheater integrated with the dispensing nozzle.

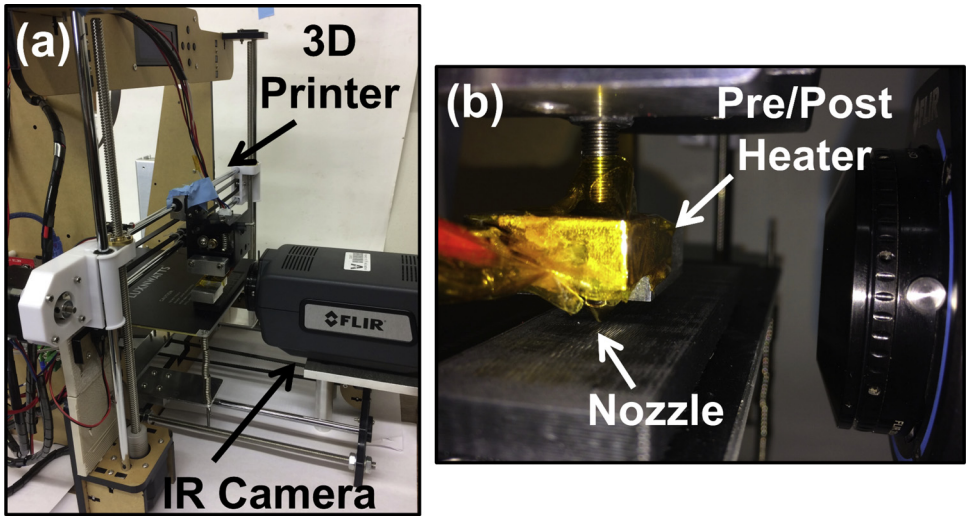

Fig. 2. (a) Picture of the experimental setup, (b) Zoom-in showing the nozzle, preheater and IR camera lens.

The standard metal heater block surrounding the nozzle is replaced with a custom-built metal heater block containing the additional preheater element. An Aluminum block is machined and integrated with the nozzle assembly in order to obtain the preheater/postheater configuration, as shown in the schematic and picture in Figs. 1(a) and 1(b) respectively. A threaded hole is drilled in the metal block in order to accommodate the nozzle assembly, which contains an embedded 40 W cartridge heater and a thermistor for temperature measurement. Thermistor reading is used by the A1284 mainboard to control the heating current going into the heater in order to maintain a constant temperature in the nozzle block as well as preheater block. Due to the high thermal conductivity of aluminum, the entire block is expected to be at the set temperature, which is validated through temperature measurement using an external thermocouple at the start of experiments. All experiments are carried out at a nozzle/heater block temperature of 205 °C. The metal block is 30 mm in length. The bottom surface of the preheater block is located just above the nozzle tip. Two different preheater samples with gaps of 0.6 mm and 1.6 mm between the bottom surface of the preheater block and nozzle tip are built. The nozzle tip is always placed 0.35 mm above the surface on which filament is dispensed, so that the bottom surface of the preheater block is 0.95 mm and 1.95 mm above the surface for the two preheater samples respectively. Filaments are dispensed on a pre-fabricated PLA block.

Note that when the nozzle-heater assembly shown in Figs. 1(a) and 1(b) moves from left to right while dispensing filament, the metal block moves ahead of the dispensing nozzle, and therefore acts as a preheater. On the other hand, nozzle motion from right to left results in the block acting as a postheater that heats up the filament after dispense. In addition, a combined pre/post-heater is also fabricated by bolting together two separately machined Aluminum parts. This allows simultaneous heating both before and after filament dispense.

For reference, a baseline process using only the conventional nozzle assembly is also carried out. Experiments are carried out at multiple print speeds of 2.7, 4.1, 10.4 and 21.6 mm/s for both 0.95 mm and 1.95 mm gap configurations.

The infrared camera in these experiments measures infrared emission in the 3.0-5.0 μm wavelength range. The measured radiation field is converted to temperature field through the emissivity of the surface being measured. The camera is placed around 5 cm from the field of view, in which, the hot moving nozzle dispenses the new PLA layer. The temperature field is measured at a rate of 30 frames per second. Since the accuracy of infrared-based temperature measurement depends critically on the quality of calibration, an extensive calibration is carried out in advance of the experiments. The infrared camera is used to measure the temperature of a PLA sample maintained at a number of well-known temperatures using an Instec HCS622 V thermal stage. The emissivity of PLA is determined as the value that results in best agreement between the known set temperatures and measured temperatures by the infrared camera in these calibration measurements. The determined emissivity of 0.92 is used throughout the experiments.

Experiments are also carried out to investigate the effect of heating on the mesostructure of the filaments, and thermal and mechanical properties of the printed sample. For measurement of thermal properties, samples of size 40 mm by 40 mm and a number of thicknesses are printed with combined preheater and postheater configuration at 1.95 mm gap, as well as the no-heater, baseline case. In order to reveal the filament cross-section in each case, the printed samples are cut using liquid Nitrogen as described in a recent paper [21]. Briefly, the samples are dipped in liquid Nitrogen for 10 min, followed by impact load on a notch, which results in a clean cut of the sample without blurring of the cross-section that would have occurred in case of a heat-generating cutting process such as sawing. Thermal resistance of printed samples is measured using a one-dimensional heat flux method, in which the sample is sandwiched between two plates maintained at different temperatures, and thermal resistance is determined through measurement of heat flux through the sample resulting from the temperature difference.

Dogbone samples for measurement of tensile properties are printed with baseline, no-heater settings and with combined preheater-postheater with 0.95 mm gap between the base and heater surface. Test coupons are built based on a modified version of ASTM D638-2a 'Standard Test Method for Tensile Properties of Plastics' [27]. Test coupons are 73.68 mm long, 12 mm wide and 3.2 mm thick. Standard print process settings are used, and the print speed is chosen to be 33.3 mm/s. Length, width and thickness of the test coupons are aligned with X, Y and Z axes with respect to the build plate. Tensile testing is carried out on a Shimadzu AGS-X series universal test frame with a high-precision 5 kN load cell. The cross-head speed is set at 0.02 mm/min. All tests are conducted in stroke-controlled mode. Samples are gripped using a pair of mechanical grips. No grip failure is observed. Load and displacement data are collected using a standard data acquisition system, and post-processed to obtain stress-strain curves.

3. Analytical and numerical modeling

Temperature rise in previously deposited layers during the deposition of a new filament layer occurs due to two distinct heat sources [17]. The first mechanism is the diffusion of thermal energy contained

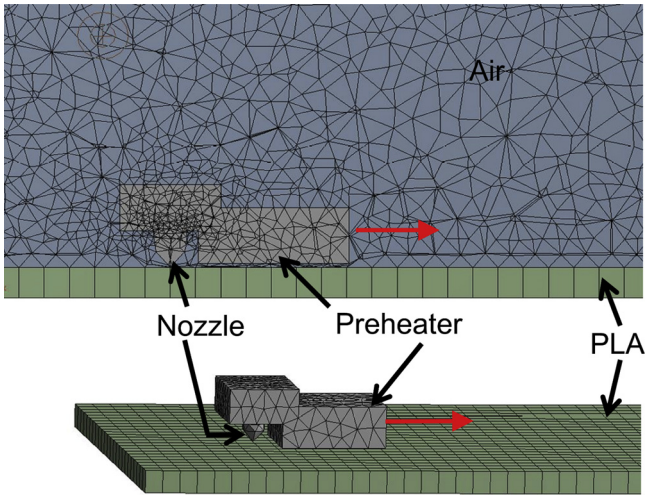

Fig. 3. Finite-volume simulation setup showing the geometry and meshing.

in the hot dispensed filament. Further, heat transfer also occurs from the hot nozzle through the small air gap into the bed. The latter is a potentially dominant mechanism due to the close promixity between the bed and the rastering nozzle. Similar to heating due to hot nozzle, the presence of the hot preheater or postheater in these experiments is expected to contribute towards temperature rise. As a result, two distinct approaches are taken for modeling the contributions of these mechanisms towards temperature rise on the previous deposited layer. The effect of thermal energy of the dispensed filament is modeled using a well-known analytical equation, whereas heat transfer from the hot nozzle and pre/post-heater is quantified through a finite-volume simulation model.

3.1. Analytical modeling for effect of filament dispense

The theoretical treatment discussed in a recent paper [17] is utilized for modeling the effect of hot filament dispense on the temperature distribution. Based on well-known theory of moving heat sources [28,29], temperature distribution due to diffusion of thermal energy in the hot deposited filament is computed by analyzing the problem in a coordinate system that travels along with the moving nozzle. By solving the governing energy conservation equation subject to appropriate boundary conditions, temperature distribution along the raster line can be shown to be [17]

$$T = T_o + \frac{\dot{q}}{2\pi k \cdot |x - u_x t|} exp\left[-\frac{u_x(|x - u_x t| + x - u_x t)}{2\alpha}\right] \quad (1)$$

where T_0 is the ambient temperature, u_x is the nozzle speed in the x direction, k and α are thermal conductivity and thermal diffusivity respectively. $\dot{q}$ is the rate at which thermal energy is deposited along with the filament, given by [17]

$$\dot{q} = \int_{T_0}^{T_n} \dot{m} C_p dT \quad (2)$$

where $\dot{m}$ is the mass flow rate, C_p is the filament heat capacity and T_n is the nozzle temperature.

3.2. Finite-volume modeling

Due to the geometrical complexity of the nozzle and pre/postheater assembly, it is difficult to derive an analytical equation for heat transfer into and subsequent temperature rise of the previously deposited filament layers. A finite-volume simulation model is developed to account for these effects. These simulations are carried out in ANSYS Fluent, where the motion of the nozzle and pre/post-heater assembly is simulated using dynamic mesh motion. A new mesh is generated at each time step as the nozzle and pre/post-heater move through the ambient air, resulting in geometrical changes over time. In this case, the motion is described simply by a linear velocity.

A simulation model of the geometry, including the nozzle and pre/post-heater assembly, PLA base and ambient air is created. The nozzle and pre/post-heater are maintained at a fixed temperature of 205 °C, consistent with experimental conditions. Initial temperature of the PLA base is set at 30 °C. Convective heat transfer boundary conditions are applied on the sides of the PLA base, with a convection coefficient of 10 W/m^{2}K, consistent with natural convection conditions in experiments.

Motion of the nozzle and pre/postheater assembly is implemented using a user-defined function that specifies constant speed rigid body motion in the x direction. Dynamic layering mesh motion method is utilized for temperature computation. It is ensured that boundary displacement between successive timesteps is much smaller than local cell sizes in order to avoid cell degeneration and negative cell volume. At each timestep, local remeshing is carried out for each cell that is significantly affected by the rigid body motion, for example due to excessive skewing or exceeding the limits of minimum and maximum size criteria. Fig. 3 presents pictures of the finite volume model, showing the nozzle, preheater, PLA layer underneath and ambient air. As shown, the mesh is designed to be particularly fine around the nozzle and preheater in order to accurately account for heat transfer in the thin layer of air.

4. Results and discussion

4.1. Effect of preheater and postheater configurations on temperature distribution

The effect of preheater and postheater configurations on temperature distribution along the raster line is studied through a number of experiments.

Fig. 4(a) presents temperature measurement at a fixed location on the raster line as a function of time in the preheater configuration,

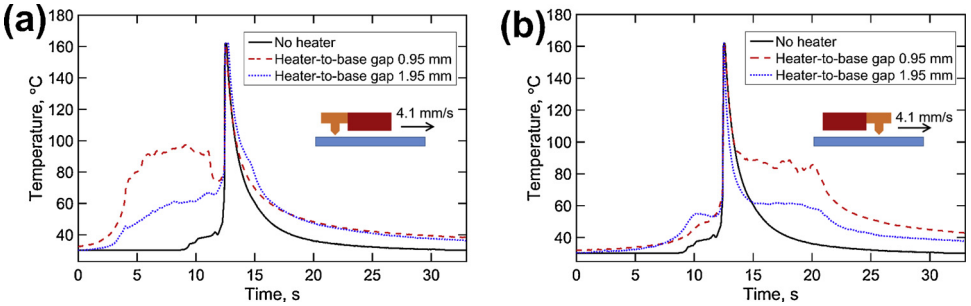

Fig. 4. Measured temperature as a function of time at a fixed point on the raster line for two different heater-to-base gaps. For reference, the baseline case without additional heating is also shown. (a) and (b) show data for preheater and postheater configurations, respectively.

wherein the hot metal block travels ahead of the dispensing nozzle in the preheater configuration. Temperature is plotted for two different heater-to-base gaps – 0.95 mm and 1.95 mm – at a fixed raster speed of 4.1 mm/s. For comparison, temperature measurement corresponding to the baseline case without preheating at the same raster speed is also plotted. In each of the three cases plotted in Fig. 4(a), temperature rises slowly as the nozzle approaches the point of interest, followed by a sharp rise and peak at the time when the filament is dispensed at the point of interest. Subsequently, there is a gradual decline in temperature as the nozzle moves away from the point of interest. These characteristics are all consistent with measurements reported in the past, as well as with theoretical predictions from moving heat source theory [17].

The impact of the preheater configuration is seen clearly in the two plots corresponding to preheater configurations in Fig. 4(a). Both show significant increase in temperature even prior to arrival of the nozzle. The two plateaus in Fig. 4(a) correspond to additional preheating caused by the preheater configuration that arrives at the point of interest prior to the nozzle. After the nozzle has passed the point of interest, temperature reduces for all three cases following the same general trend. There is some additional temperature increase in the two curves corresponding to the preheater configurations compared to the baseline, which is likely due to diffusion of thermal energy absorbed from the preheater even before nozzle arrival.

Further, Fig. 4(a) shows that the temperature increase due to preheater configuration is a function of the heater-to-base gap. In the two cases studied here, the lower gap results in higher temperature rise, which is along expected lines because of increased conduction and radiation heat transfer between the hot preheater surface and the raster plane. Conduction heat transfer increases due to increased temperature gradient, whereas radiative heat transfer increases due to increased radiative view factor between the two surfaces at lower gap. Fig. 4(a) provides evidence of enhanced temperature rise due to the preheater configuration, which may be expected to result in increased filament-to-filament bonding.

Similar experiments are then carried out to understand the thermal impact of postheater configuration. A fixed raster speed of 4.1 mm/s and heater-to-base gaps of 0.95 mm and 1.95 mm are utilized, similar to Fig. 4(a). Postheater configuration data are plotted in Fig. 4(b), along with a baseline case with no additional heating. The impact of the postheater configuration on temperature distribution after filament dispense is clearly seen in Fig. 4(b). There is greater temperature rise for the lower gap case, as expected, due to greater rate of conduction and radiative heat transfer enabled by the small gap. The postheater configuration does not significantly impact temperature before filament dispense, because minimal heat transfer is expected at the point of interest until the nozzle has passed and the postheater appears above the point. This is similar to the preheater configuration case, where there was relatively lower impact on temperature after filament dispense.

To further understand the thermal impact of preheater and postheater configurations, experiments are carried out for the two configurations at multiple raster speeds. Fig. 5(a) plots temperature as a function of time at a fixed point on the raster line for the preheater configuration at three different raster speeds. The heater-to-base gap is fixed at 0.95 mm. Measurement for the baseline case without preheating is also plotted for comparison. Similar to Fig. 4(a), at each raster speed, a significant temperature plateau is observed prior to the peak, while the peak temperature does not change much. The area under the temperature-time curve, which roughly corresponds the total thermal dose, or energy, transferred into the previous deposited layers is significantly increased by the use of the preheater, particularly at low raster speeds. This is because at low raster speed, the point of interest is exposed to the hot preheater surface for a longer time, which results in a greater width of the plateau region in Fig. 5(a) prior to the temperature peak. This indicates that a lower raster speed may result in greater duration of elevated temperature prior to filament dispense. The width of this region in all three cases is found to be close to the expected value based on the raster speed in each case and the physical width of the preheater. Following the temperature peak at the time of filament dispense, temperature reduces gradually, with greater deviation between the two cases at lower raster speeds. This is likely due to greater thermal energy absorbed in the greater time of exposure at lower raster speeds.

Fig. 5(b) plots experimental data from similar experiments in the postheater configuration at three different raster speeds. As expected, in these cases, increased temperature rise is observed after the nozzle has passed over the point of interest, because in this case, the postheater trails behind the nozzle and heats up the point of interest after filament dispense. Similar to Fig. 4(b), relatively lesser impact is observed before filament dispense, and similar to Fig. 5(a), elevated plateau in the temperature plot after filament dispense is found to be the widest for the lowest raster speed investigated in these experiments.

Finally, these experiments are carried out for a combined preheater-postheater configuration. A comparison of the combined configuration with preheater-only and postheater-only is presented in Fig. 6(a) and (b) for two different raster speeds. These plots show that the presence of both configurations results in significant increase in temperature at the point of interest both before and after filament dispense. The preheater-postheater configuration offers the benefits of both individual configurations. As expected, time duration for which increased temperature is observed is lower for higher raster speed (Figs. 6(a) vs. 6(b)), which is explained by the shorter exposure time at higher raster speed. The provisioning of both preheating and postheating configurations incurs only minor increase in cost and complexity compared to only one. The heating current is expected to go up nominally due to the increased thermal mass to be maintained at a high temperature, but otherwise, this represents a very passive approach for obtaining significant benefits in filament-to-filament bonding.

4.2. Analytical/numerical model results and comparison with experimental measurements

Experimental measurements are compared with analytical and numerical models discussed in section 3 that predict temperature distribution at the interface of previous and newly deposited layer. These models account for temperature rise due to two independent effects

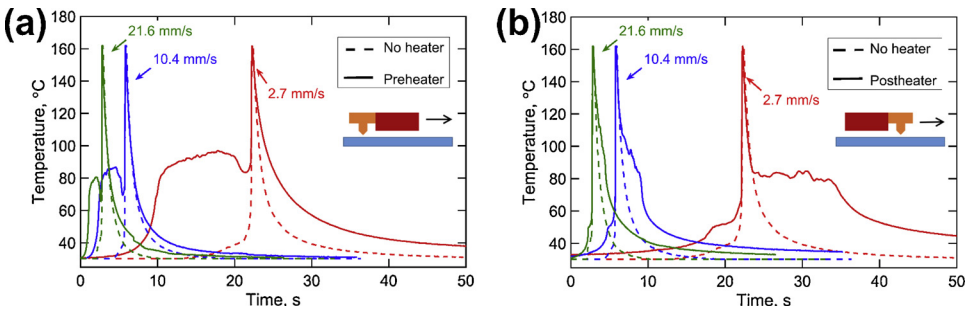

Fig. 5. Measured temperature as a function of time at a fixed point on the raster line for three raster speeds. For reference, the baseline case without additional heating is also shown. (a) and (b) show data for preheater and postheater configurations, respectively. Broken and solid lines correspond to the baseline and heater cases respectively, while colors correspond to three different raster speeds.

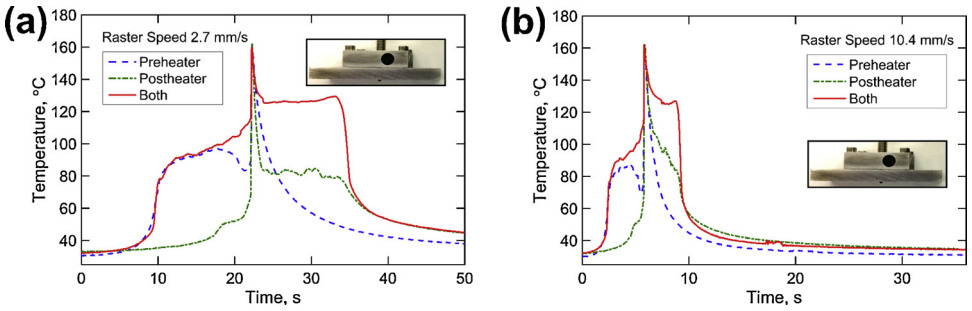

Fig. 6. Temperature plots comparing the impact of preheater and postheater configurations with a case where both preheater and postheater are used. (a) and (b) show these plots for raster speeds of 2.7 mm/s and 10.4 mm/s respectively.

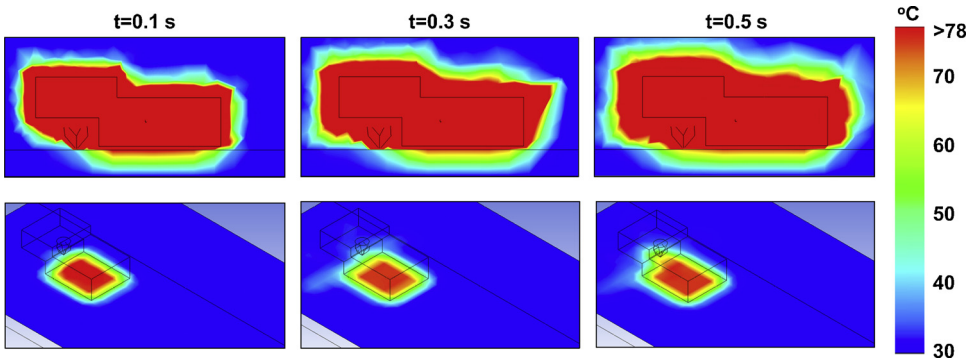

Fig. 7. Colorplots showing temperature distribution predicted by the finite-volume simulation at three different times while the nozzle-preheater assembly rasters along a straight line.

separately – thermal energy in the deposited filament and heat transfer from the hot nozzle and pre/post heaters. While a previously reported analytical model [17] is used for computing the effect of thermal energy in the deposited filament, a finite-volume simulation model is used to account for the effect of the hot nozzle and pre/post heaters due to the considerable geometrical complexity. Fig. 7 presents colorplots of the temperature distribution predicted by the finite-volume simulation model at three different times while the nozzle-preheater assembly rasters along a straight line from left to right. While one set shows a cross-section view, the other set shows the temperature profile on the base surface in an isometric view while showing only an outline of the preheater and nozzle assembly. These plots clearly show the thermal influence of the preheater. Temperature on the base surface directly underneath the preheater block is significantly elevated. While the thermal impact of the preheater block does not extend much beyond its footprint, the effect is highly directed and heats up precisely the region at which the filament is about to be dispensed. Further, the size of the preheater block can potentially be changed in order to change the size of the zone of thermal influence. As the preheater-nozzle assembly moves from left to right, the heated zone on the base surface also moves. The preheater effectively preheats the base surface before filament is dispensed, which may be very effective for promoting filament-to-filament adhesion.

Fig. 8 present comparison between experimental measurements and analytical/numerical model. Thermal conductivity, specific heat and density of the PLA platform are taken to be 0.2 W/mK, 1800 J/kgK and 1300 kg/m^3. The nozzle and preheater block are assumed to be maintained at 205 °C. Heat transfer due to convective motion in the ambient air is neglected. Fig. 8 plots experimentally measured and theoretically predicted temperature distribution along the raster line at two different times for fixed heater-to-base gap of 0.95 mm and raster speed of 10.4 mm/s. In both cases, there is good agreement between measurements and modeling. As shown, the theoretical model predicts infinite temperature at the location of the filament due to the presence of a singularity at $x = u_x \cdot t$ in Eq. (1), which is the reason behind the

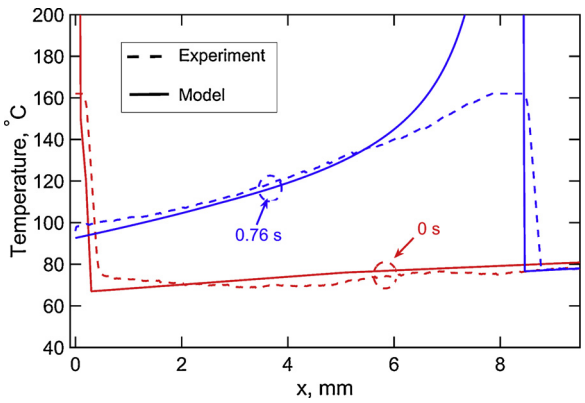

Fig. 8. Comparison of experimental temperature measurement along the raster line on the bed surface with predictions based on the analytical and finite-element simulation models. Temperature profile is plotted at two different times for the case of dispensing with preheater.

deviation close to the location of the filament. Several possible sources of error exist in both experiments and modeling. For example, the finite-volume model does not account for microscale surface finish of the heater that may play an important role in heat transfer across the small gap. The simulation model does not account for radiative heat transfer across the air gap. Further, the model assumes the filament deposition process to deposit a point source of heat, whereas in experiments, the heat source is likely to be somewhat more distributed. Finally, measurement errors associated with infrared thermometry may also exist. Within the limitations of these sources of error, Fig. 8 represents good agreement between measurements and modeling.

4.3. Effect of pre/post heating on filament interlayer bonding

The key motivation behind the design of the preheater and

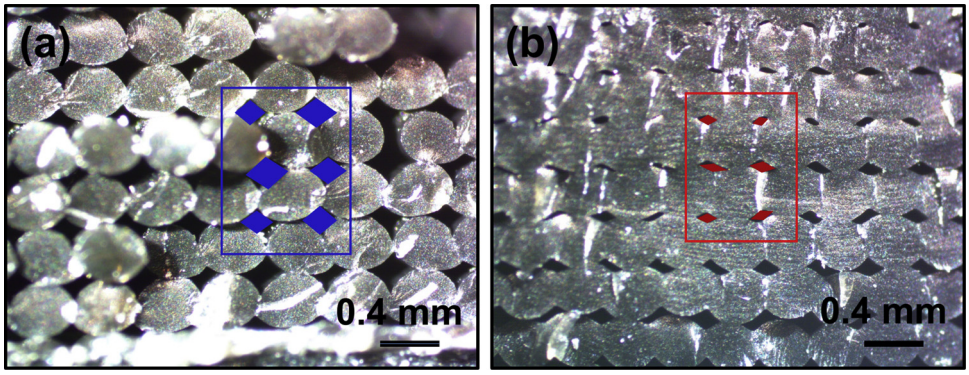

Fig. 9. Cross-section images showing the impact of combined pre/post heating on filament-to-filament bonding. (a) shows the baseline case, while (b) shows the case with pre/post heating. In this case, the raster speed is 60 mm/s and heater-to-base gap is 0.95 mm.

postheater configurations is to supply additional thermal energy to the raster lines, and therefore increase the effectiveness of merging between adjacent filaments. While Figs. 4–8 clearly present evidence of increased temperature along the raster line due to the preheat and postheater configurations, further experiments are also carried out to investigate the effect of this temperature rise on the filament mesostructure and eventually on functional properties of the printed parts.

Fig. 9 presents cross-section images for the baseline case and for a combined preheater-postheater configuration at 60 mm/s raster speed and 0.95 mm gap from the heater surface and base. These images clearly show evidence of increased filament-to-filament necking (i.e. increase in negative gap between adjacent filaments) due to the thermal effect of the preheater and postheater configurations. In order to estimate the fraction of voiding in the baseline and combined preheater-postheater samples, representative void spaces in Fig. 9 are filled with variable size diamonds of known area. The sum of the diamond-occupied area represents the approximate area of voids. Table 1 outlines the calculated area fraction of the voided area in the two samples. These data show significant reduction in the fraction of void area from 0.230 in the baseline samples to 0.067 in the combined preheater-postheater sample.

Further, Fig. 10 plots measured thermal resistance of printed samples as a function of sample thickness for both baseline samples without heater, as well as samples printed with a combined preheater-postheater. Data clearly show significant reduction in values of thermal resistance as well as the slope as a result of the combined preheater-postheater. Based on the reduced slope, the combined preheater-postheater results in around 22% increase in thermal conductivity. The improvement correlates well with the improved filament-to-filament bonding shown in Fig. 9, since it is well-known that interfacial thermal transport between filaments plays a key role in determining overall thermal performance of the part [10]. The significant improvement in thermal performance demonstrated here may be critical for applications where the part is expected to withstand thermal loads.

Finally, Fig. 11 plots stress-strain curves for a baseline sample and a combined preheater-postheater sample, both printed at 33.3 mm/s speed. The resulting mechanical properties are also summarized in Table 2, showing 60% and 165% improvement in Ultimate Tensile Stress and Modulus of Toughness, respectively. Such improvement arises directly from improved filament-to-filament bonding and

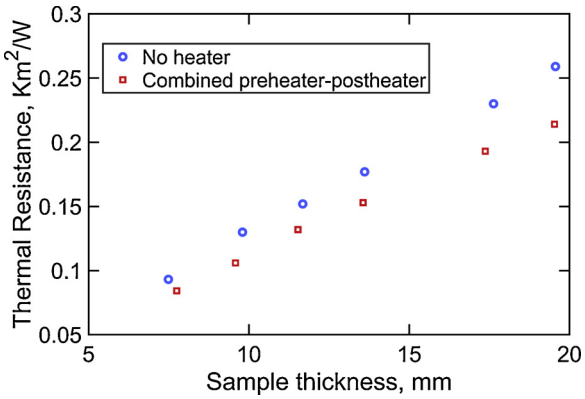

Fig. 10. Variation of measured thermal resistance of printed samples with sample thickness. Data are presented for both baseline samples as well as those printed with combined pre-heater and post-heater. Reciprocal of the slope of the curves is indicative of thermal conductivity of the samples.

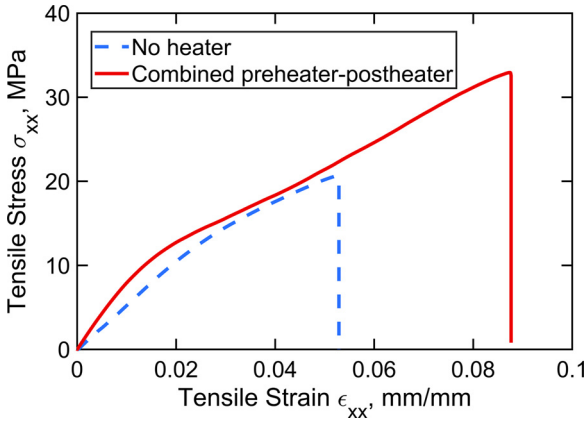

Fig. 11. Stress-vs-strain plot for samples printed at 3600 mm/min scan speed for both baseline case and with preheater-postheater configuration, showing significant improvement in strength and toughness.

reduced void area fraction as shown in Fig. 9. This is consistent with recent work [30] that shows 85% reduction in stress intensity of

Table 1
Estimated area fraction of the voided area in the baseline no-heater and combined preheater-postheater samples.

Sample Type	Area of Representative Volume Element (cm^2), A_R	Area of Void (cm^2), A_V	Void Area Fraction, v_{void}
No Heater	9.9	2.28	0.230
Combined Preheater-postheater	6.5	0.44	0.067

Table 2
Measured mechanical properties of the baseline no-heater and combined preheater-postheater samples. The percentage improvement for each property is listed within brackets.

Sample Type	Young's modulus, E (MPa)	Ultimate tensile strength (MPa)	Modulus of Toughness (kPa)
No Heater	512	20.6	625
Combined preheater-postheater	844 (65%)	32.9 (60%)	1655 (165%)

singularity points between adjacent filaments due to an increase in filament-to-filament gap setting from 0.1% to 1%. The 164% increase in modulus of toughness also supports the premise of improved filament-to-filament bonding due to preheater and postheating.

While experiments carried out in this work make a distinction between preheater and postheater configurations because only a single filament line is being rastered, it must be recognized that such a distinction may not exist in practical scenarios where multiple lines are being sequentially rastered. This is because typically the nozzle travels in a U configuration, so that when one line is rastered from left to right, the next is rastered from right to left. This results in the preheater configuration in the first line effectively acting as a postheater configuration in the next line when the travel direction of the nozzle reverses. Therefore, it is expected that even a single metal heater may result in combined preheater/postheater effects. Due to the simplicity of the design of the heating mechanism studied here compared to past efforts for external heating [24–26], it is certainly possible to include both preheater and postheater configurations, such as shown in the inset of Fig. 6, in order to maximize the thermal benefit without much incremental cost or effort.

5. Conclusions

This work investigates a novel technique for providing additional heating to previously deposited layers in polymer additive manufacturing. This technique utilizes a hot metal block rastering ahead of and/or behind the dispensing nozzle, and is much simpler compared to past approaches such as laser heating or microwave heating. Infrared thermography clearly shows the significant impact of this approach on the temperature distribution in the previously deposited layer. A combined approach that integrates both preheater and postheater configurations may be of particular interest as it combines the thermal benefits of both configurations with minimal additional cost or complexity. Experimental data are shown to be in good agreement with modeling results. The increased thermal energy into the part is shown to have a positive impact on the filament mesostructure, as well as thermal/mechanical properties.

This approach can potentially be used for improving thermal and mechanical properties of parts built using polymer AM processes. Through careful process optimization, this may result in parts with novel thermal and mechanical properties that are not possible through conventional polymer AM processes.

References

[1] D. Dimitrov, K. Schreve, N. de Beer, Advances in three dimensional printing – state of the art and future perspectives, Rapid Prototyping J. 12 (2006) 136–147.
[2] I. Zein, D.W. Hutmacher, K.C. Tan, S.H. Teoh, Fused deposition modeling of novel scaffold architectures for tissue engineering applications, Biomaterials 4 (2000) 1169–1185.
[3] P. Vojislav, V.H.G. Juan, J.F. Olga, D.G. Javier, R.B.P. Jose, P.G. Luis, Additive layered manufacturing: sectors of industrial application shown through case studies, Int. J. Mech. Prod. Eng. Res. Dev. 49 (2010) 1061–1079.
[4] S. Bose, S. Vahabzadeh, A. Bandyopadhyay, Bone tissue engineering using 3D printing, Mater. Today 12 (2013) 496–504.
[5] S. Thompson, Z. Aspin, N. Shamsaei, A. Elwany, L. Bian, Additive manufacturing of heat exchangers: a case study on a multi-layered Ti–6Al–4V oscillating heat pipe, Addit. Manuf. 8 (2015) 163–174.
[6] Q. Sun, G. Rizvi, C. Bellehumeur, P. Gu, Effect of processing conditions on the bonding quality of FDM polymer filaments, Rapid Prototyp. J. 14 (2008) 72–80.
[7] D. Ravoori, L. Alba, H. Prajapati, A. Jain, Investigation of process-structure-property relationships in polymer extrusion based additive manufacturing through in situ high speed imaging and thermal conductivity measurements, Addit. Manuf. 23 (2018) 132–139.
[8] B.M. Tymrak, M. Kreiger, J.M. Pearce, Mechanical properties of components fabricated with open-source 3-D printers under realistic environmental conditions, Mater. Des. 58 (2014) 242–246.
[9] S. Ahn, M. Montero, D. Odell, S. Roundy, P.K. Wright, Anisotropic material properties of fused deposition modeling ABS, Rapid Prototyp. J. 8 (2002) 248–257.
[10] H. Prajapati, D. Ravoori, R. Woods, A. Jain, Measurement of anisotropic thermal conductivity and inter-layer thermal contact resistance in polymer fused deposition modeling (FDM), Addit. Manuf. 21 (2018) 84–90.
[11] A. D'Amico, A.M. Peterson, An adaptable FEA simulation of material extrusion additive manufacturing heat transfer in 3D, Addit. Manuf. 21 (2018) 422–430.
[12] C. Duty, C. Ajinjeru, V. Kishore, B. Compton, N. Hmeidat, X. Chen, P. Liu, A. Hassen, J. Lindahl, V. Kunc, What makes a material printable? A viscoelastic model for extrusion-based 3D printing of polymers, J. Korean Soc. Manuf. Process. Eng. 35 (2018) 526–537.
[13] S.F. Costa, F.M. Duarte, J.A. Covas, Estimation of filament temperature and adhesion development in fused deposition techniques, J. Mater. Processing Technol. 245 (2017) 167–179.
[14] A. Costa, A. da Silva, O. Carneiro, A study on extruded filament bonding in fused filament fabrication, Rapid Prototyp. J. (2018), https://doi.org/10.1108/RPJ-03-2018-0062).
[15] J. Yin, C. Lu, J. Fu, Y. Huang, Y. Zheng, 'Interfacial bonding during multi-material fused deposition modeling (FDM) process due to inter-molecular diffusion,', J. Mater. Des. 150 (2018) 104–112.
[16] C. Bellehumeur, L. Li, Q. Sun, P. Gu, Modeling of bond formation between polymer filaments in the fused deposition modeling process, J. Korean Soc. Manuf. Process. Eng. 6 (2004) 170–178.
[17] D. Ravoori, C. Lowery, H. Prajapati, A. Jain, Experimental and theoretical investigation of heat transfer in platform bed during polymer extrusion based additive manufacturing, Polym. Test. 73 (2019) 439–446.
[18] B.G. Compton, B.K. Post, C.E. Duty, L. Love, V. Kunc, Thermal analysis of additive manufacturing of large-scale thermoplastic polymer composites, Addit. Manuf. 17 (2017) 77–86.
[19] H. Prajapati, D. Ravoori, A. Jain, Measurement and modeling of filament temperature distribution in the standoff gap between nozzle and bed in polymer-based additive manufacturing, Addit. Manuf. 24 (2018) 224–231.
[20] J.E. Seppala, K.D. Migler, Infrared thermography of welding zones produced by polymer extrusion additive manufacturing, Addit. Manuf. 12 (2016) 71–76.
[21] H. Prajapati, D. Chalise, D. Ravoori, A. Jain, Improvement in build-direction thermal conductivity in extrusion-based polymer additive manufacturing through thermal annealing, in review, Addit. Manuf. (2019), https://doi.org/10.1016/j.addma.2019.01.004.
[22] K.R. Hart, R.M. Dunn, J.M. Sietins, C.M.H. Mock, M.E. Mackay, E.D. Wetzel, 'Increased fracture toughness of additively manufactured amorphous thermoplastics via thermal annealing,', Polymer 144 (2018) 192–204.
[23] M.D. Wolkowicz, S.K. Gaggar, Effect of thermal aging on impact strength acrylonitrile-butadiene-styrene (ABS) terpolymer, Polym. Eng. Sci. 21 (1981) 571–575.
[24] A. Ravi, A. Deshpande, K. Hsu, An in-process laser localized pre-deposition heating approach to inter-layer bond strengthening in extrusion based polymer additive manufacturing, J. Korean Soc. Manuf. Process. Eng. 24 (2016) 179–185.
[25] V. Kishore, C. Ajinjeru, A. Nycz, B. Post, J. Lindahl, V. Kunc, C. Duty, Infrared preheating to improve interlayer strength of big area additive manufacturing (BAAM) components, Addit. Manuf. 14 (2017) 7–12.
[26] C. Sweeney, B. Lackey, M. Pospisil, T. Achee, V. Hicks, A. Moran, B. Teipel, M. Saed, M. Green, Welding of 3D-printed carbon nanotube–polymer composites by locally induced microwave heating, Sci. Adv. 6 (2017) 1–6.
[27] https://www.astm.org/Standards/D638.htm, last accessed May 28, 2019.
[28] D.W. Hahn, M.N. Özişik, 'Heat Conduction,', third ed., John Wiley & Sons, Hoboken, New Jersey, 2012.
[29] E. Kannatey-Asibu Jr., 'Principles of Laser Materials Processing', 1st ed., John Wiley & Sons, 2009.
[30] A. Rezaee, A. Adnan, On the elastic stress singularities and mode I notch stress intensity factor for 3D printed polymers, Eng. Fract. Mech. 204 (2018) 235–245.